On the control of surface waves by a vertical magnetic field

Binod Sreenivasan
Department of Mathematical Sciences, University of Exeter, North Park Road, Exeter EX4 4QE, United Kingdom

Peter A. Davidson
Department of Engineering, University of Cambridge, Trumpington Street, Cambridge CB2 1PZ, United Kingdom

Jacqueline Etay
CNRS-EPM, ENSHMG, BP 95, 38402 St Martin d'Hères Cedex, France

(Received 11 January 2005; accepted 20 September 2005; published online 1 November 2005)

We consider the magnetic damping of surface gravity waves by a vertical magnetic field. The damping mechanism is, in principle, quite simple. The motion of a conducting fluid in the presence of an imposed magnetic field leads to electric currents, and hence to Ohmic dissipation. As the fluid heats up, there is a corresponding loss in the mechanical energy of the wave motion. When the fluid is infinite in the horizontal plane, or else bounded by perfectly conducting vertical walls, the induced currents have a simple spatial distribution and so the analysis of such waves is straightforward [L. E. Franekel, J. Fluid. Mech. **7**, 81 (1959); P. Rivat, J. Etay, and M. Garnier, Eur. J. Mech. B/Fluids **10**, 537 (1991)]. However, in most practical applications of magnetic damping the fluid is bounded by nonconducting vertical walls. This leads to a complex distribution of electric currents and to a much weaker form of damping. In this paper, we extend the simple classical theory to accommodate nonconducting sidewalls, and show that the characteristic damping time increases by a factor of ~30 due to the presence of these walls. Experiments are described for both conducting and insulating sidewalls. The results of the experiments are in good agreement with the theory. © *2005 American Institute of Physics*. [DOI: 10.1063/1.2118708]

I. INTRODUCTION

A. The damping of motion by an imposed magnetic field

Magnetic fields are commonly used to suppress unwanted motion in electrically conducting fluids, for example, in continuous casting of steel and aluminum; see Davidson.[1] The mechanism is straightforward. Let $\mathbf{B}_0$ be a uniform magnetic field that is imposed on an incompressible fluid. The magnetic Reynolds number, $R_m=ul/\lambda$, is invariably small in such applications, and so Ohm's law and the Lorentz force experienced by the fluid simplify to (Davidson[2])

$$\mathbf{J}=\sigma(-\nabla V+\mathbf{u}\times\mathbf{B}_0), \tag{1}$$

$$\mathbf{F}=\mathbf{J}\times\mathbf{B}_0. \tag{2}$$

Here σ and λ are the electrical conductivity and magnetic diffusivity of the fluid, $\mathbf{u}$ is the velocity field, and $\mathbf{J}$ is the induced current density. Both $\mathbf{J}$ and $\mathbf{u}$ are solenoidal. Also, V is the electrostatic potential, which is determined by the divergence of Eq. (1) in the form

$$\nabla^2 V=\mathbf{B}_0\cdot\boldsymbol{\omega}, \quad \boldsymbol{\omega}=\nabla\times\mathbf{u}. \tag{3}$$

It follows that the Lorentz force is given by

$$\mathbf{F}=\sigma(\mathbf{B}_0\times\nabla V)-\sigma B_0^2\mathbf{u}_\perp, \tag{4}$$

where $\mathbf{u}_\perp$ represents the components of $\mathbf{u}$ in the plane normal to $\mathbf{B}_0$. We shall return to Eq. (4) in a moment. First, let us consider the rate of working of $\mathbf{F}$. From Eqs. (1) and (2), we have

$$\mathbf{F}\cdot\mathbf{u}=\mathbf{u}\cdot(\mathbf{J}\times\mathbf{B}_0)=-\mathbf{J}^2/\sigma-\nabla\cdot(\mathbf{J}V). \tag{5}$$

The second term on the right-hand side of (5) is a divergence that usually integrates to zero, provided there is no external source of current. Thus, we have

$$\int \mathbf{F}\cdot\mathbf{u}\,dV=-\int \mathbf{J}^2/\sigma\,dV, \tag{6}$$

which represents the conversion of mechanical energy into heat at a rate determined by the Ohmic dissipation. To determine the characteristic time scale of the process, we must return to Eq. (4). The analysis simplifies considerably in those cases where the motion is two dimensional, such as a plane wave, and when $\mathbf{B}_0$ lies in the plane of the motion. In such a situation, (3) reduces to $\nabla^2V=0$, and provided the fluid is unbounded, or else bounded by perfectly conducting walls that provide a resistance-free return path for the induced current, we may take $V=0$. Under these conditions, Eqs. (1) and (4) simplify to

$$\mathbf{J}=\sigma(\mathbf{u}\times\mathbf{B}_0), \tag{7}$$

$$\mathbf{F}=-\sigma B_0^2\mathbf{u}_\perp, \tag{8}$$

and we see that the Lorentz force acts like a linear drag acting on $\mathbf{u}_\perp$. The Navier–Stokes equation now becomes

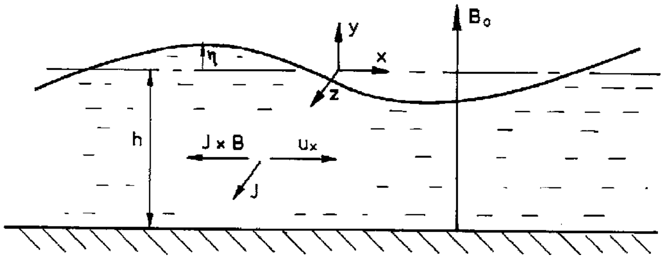

FIG. 1. A plane wave is damped by a magnetic field. The fluid is considered unbounded in the horizontal plane and the induced electric current is directed parallel to the wave crests.

$$\frac{D\mathbf{u}}{Dt} = -\boldsymbol{\nabla}\left(\frac{p}{\rho}\right) - \frac{\mathbf{u}_\perp}{\tau} + \nu\nabla^2\mathbf{u}, \tag{9}$$

where $\tau=\rho/\sigma B_0^2$ is called the magnetic damping time. For those special cases in which $V=0$, τ provides the appropriate time scale for the conversion of mechanical energy into heat.

An obvious application of (9) is the magnetic damping of plane gravity waves propagating on the surface of a pool of conducting fluid (for example, a liquid metal). In those cases where $\mathbf{B}_0$ is vertical and the pool is unbounded in the horizontal plane, V is zero and (7)–(9) apply. The determination of the corresponding wave motion is straightforward for small-amplitude waves and is documented in, for example, Fraenkel,[3] Rivat *et al.*,[4] and Shishkov.[5] We recall the analysis here, partly to place the subsequent work in context, and partly to introduce some notation.

B. Damping of a gravity wave on an infinite surface: The classical theory

Consider a pool of liquid metal bounded below by the surface $y=-h$ and with an unperturbed free surface at $y=0$, as shown in Fig. 1. We allow for small-amplitude plane waves whose wave vector is in the x direction, so that the velocity field is confined to the $x-y$ plane. The fluid is threaded by a uniform, vertical magnetic field, $\mathbf{B}_0$, and for simplicity we neglect viscous and surface tension forces. The linearized version of Eq. (9) for small-amplitude waves is

$$\frac{\partial\mathbf{u}}{\partial t} = -\boldsymbol{\nabla}\left(\frac{\delta p}{\rho}\right) - \frac{u_x\hat{\mathbf{e}}_x}{\tau}, \tag{10}$$

where δp is the perturbation in pressure from the hydrostatic distribution. We let $\eta(x,t)$ be the vertical displacement of the free surface and seek solutions of the form

$$\eta = \eta_0 \exp j(kx + \varpi t),$$

$$u_y = H(y) \exp j(kx + \varpi t),$$

$$\delta p = \rho\Pi(y) \exp j(kx + \varpi t),$$

where k and ϖ are the wave number and angular frequency. It is readily confirmed that $H(y)$ and $\Pi(y)$ satisfy the linearized boundary conditions

$$H(0) = j\varpi\eta_0, \quad H(-h) = 0, \tag{11}$$

$$\Pi(0) = g\eta_0, \tag{12}$$

which correspond to $u_y(y=0)=\partial\eta/\partial t$, $u_y(y=-h)=0$, and $\delta p(y=0)=\rho g\eta$. The divergence of Eq. (10) gives

$$\nabla^2(\delta p/\rho) = -\frac{1}{\tau}\frac{\partial u_x}{\partial x} = \frac{1}{\tau}\frac{\partial u_y}{\partial y}, \tag{13}$$

from which

$$\Pi''(y) - k^2\Pi = \frac{1}{\tau}H'(y)$$

while the vertical component of (10) requires

$$j\varpi H = -\Pi'(y). \tag{14}$$

Combining these expressions provides the governing equation for Π:

$$\Pi'' - \alpha^2\Pi = 0, \tag{15}$$

where

$$\alpha^2 = k^2\frac{j}{N+j} \tag{16}$$

and

$$N = \frac{1}{\varpi\tau} = \frac{\sigma B_0^2}{\rho\varpi}. \tag{17}$$

The quantity N is usually referred to as the interaction parameter. Finally, we solve Eq. (15) for Π, use (14) to find H, and impose boundary conditions (11) and (12). The end result is the dispersion relationship

$$\varpi^2 = \alpha g \tanh \alpha h. \tag{18}$$

Some obvious special cases arise. For example, when $N=0$ (no magnetic field), we recover the familiar expression

$$\varpi_0^2 = kg \tanh kh \tag{19}$$

while the shallow-water limit of (18) gives

$$\varpi = j/2\tau \pm \sqrt{\varpi_0^2 - (2\tau)^{-2}}. \tag{20}$$

Evidently, the wave is damped out on a time scale of τ, as anticipated earlier, and becomes critically damped when $\varpi_0\tau=1/2$. More generally, the solution of (18) as a function of $N_0=(\varpi_0\tau)^{-1}$ is shown in Fig. 2. We shall return to the dispersion relation (18) later, where we shall see that its predictions are in close agreement with experiment. However, the important point to note for the moment is that (18) was derived on the assumption that $V=0$, and this in turn requires that the free surface is infinite in extent or else the fluid is bounded by perfectly conducting vertical walls that allow the induced current

$$J = \sigma u_x B_0 \hat{\mathbf{e}}_z \tag{21}$$

to recirculate within the walls, as shown in Fig. 3. In practice, however, the more common situation is where the vertical walls are electrically insulating, and in such a situation the current paths must close within the fluid. Evidently, the electric field $-\boldsymbol{\nabla}V$ is nonzero in such a case and the analysis above is inadequate. One of our goals in this paper is to

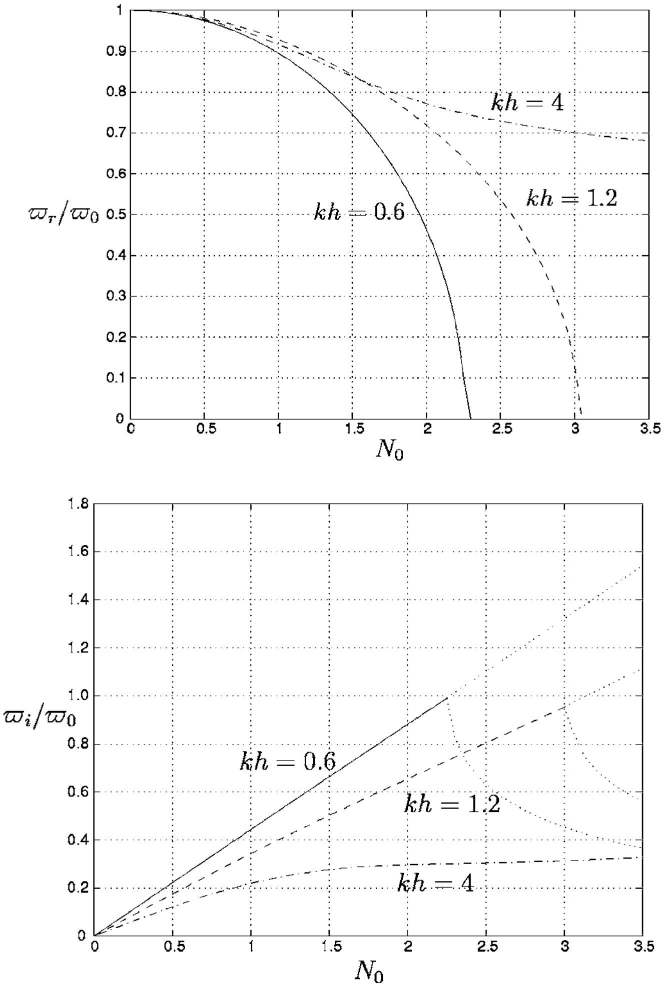

FIG. 2. Real and imaginary parts of the frequency determined by (18) as a function of the magnetic interaction parameter, N_0, shown for different values of the parameter kh. The roots of the characteristic equation in the region of $\varpi_r=0$ are shown dotted. Note that for moderate depths ($kh=0.6, 1.2$), ϖ_i/ϖ_0 is approximately linear in N_0, which is equivalent to a damping time proportional to τ.

determine the manner in which the current paths close within the fluid when the walls are insulating, and thus find the associated damping time, t_d. We shall see that, in such cases, the damping time no longer scales as $t_d \sim \tau$, but rather as

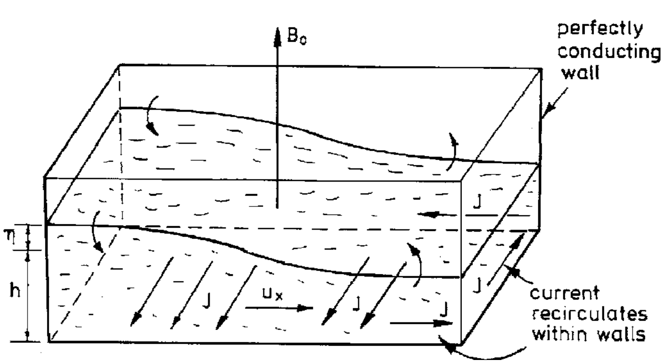

FIG. 3. When the fluid is enclosed by perfectly conducting walls, the problem is essentially that shown in Fig. 1 since the induced current is recirculated within the sidewalls and no voltage is required to drive the current through the walls. The main effect of the boundaries is to determine the wave number, k.

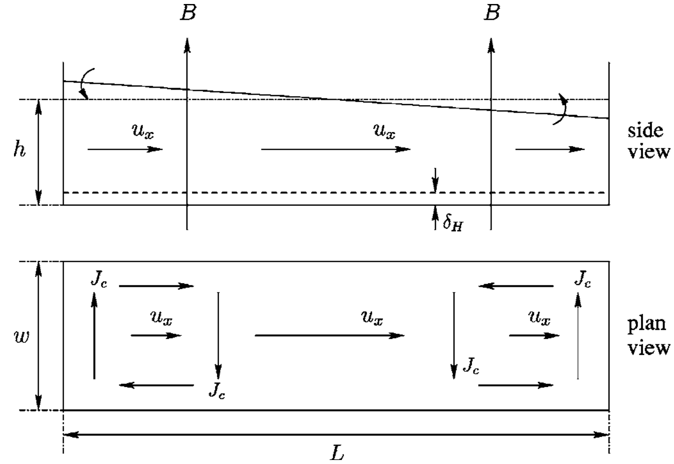

FIG. 4. Wave motion and induced current in an insulating box.

$$t_d = \frac{A\tau}{f(Ha)}, \tag{22}$$

where Ha is the Hartmann number based on the pool width, w,

$$Ha = \left(\frac{\sigma B_0^2 w^2}{\rho\nu}\right)^{1/2} = \left(\frac{w^2}{\tau\nu}\right)^{1/2}, \tag{23}$$

and f is a function of Ha, which tends to unity for large Ha. The coefficient A depends on the width, depth, and wavelength of the wave, and is typically of order 50. In the following section, we will demonstrate that, in the shallow-water limit, (22) contains no adjustable coefficients. We shall show that (22) is in close agreement with the experimental data.

II. THE CASE OF NONCONDUCTING WALLS

Let us suppose that the fluid is contained between insulating walls separated by distances L and w, as shown in Fig. 4. As before, the unperturbed fluid depth is h and we consider small-amplitude waves in which surface tension forces are neglected. To focus thoughts we consider the fundamental mode, $k=\pi/L$, although the analysis extends in an obvious way to any standing wave. (All our experiments correspond to the fundamental mode.) The coordinate system is that shown in Fig. 1. Since V is nonzero for electrically insulating walls, we must generalize the analysis of Sec. I B to allow for a nonzero electric field.

Let us start with the simplest case where viscous forces may be neglected, the pool is shallow, and Ha is small. (We shall incorporate the effects of a finite viscosity, pool depth, and Ha later.) We have

$$\rho\frac{\partial \mathbf{u}}{\partial t} = -\nabla\delta p + \mathbf{F}, \tag{24}$$

where $\mathbf{F}$ is given by Eq. (4). Now one of the curious features of (4) is that the electric potential V does not enter into the divergence of $\mathbf{F}$. That is to say, taking the divergence of (4) yields

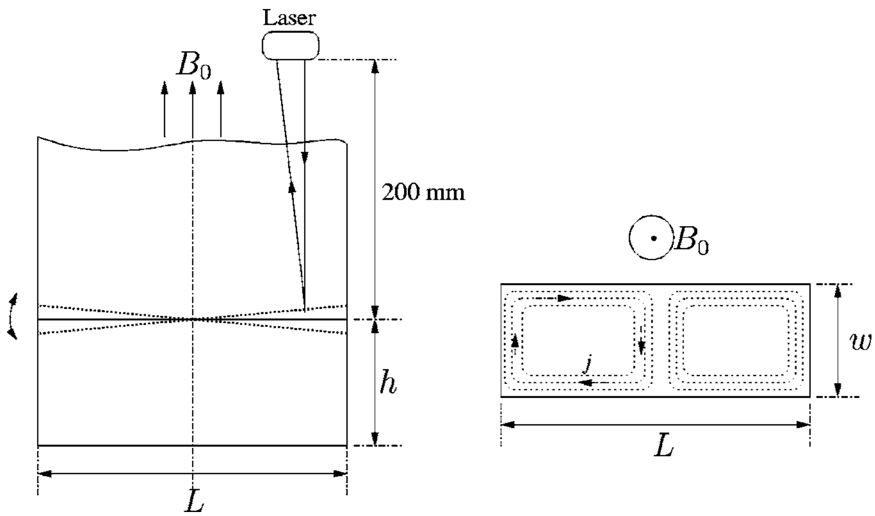

FIG. 5. Schematic of the experiment where a standing wave is generated in the presence of a vertical magnetic field, with the box cross section shown on the right. $L=150$ mm, $w=40$ mm.

$$\nabla \cdot \mathbf{F} = -(\rho/\tau)\, \nabla \cdot \mathbf{u}_\perp = (\rho/\tau)\partial u_y/\partial y,$$

which is independent of V. So, in the core, δp and u_y are governed by

$$\nabla^2\left(\frac{\delta p}{\rho}\right) = \frac{1}{\tau}\frac{\partial u_y}{\partial y}, \tag{25}$$

$$\frac{\partial u_y}{\partial t} = -\frac{\partial}{\partial y}\left(\frac{\delta p}{\rho}\right). \tag{26}$$

These may be rewritten as second-order equations for δp and u_y:

$$\frac{\partial}{\partial t}\nabla^2\left(\frac{\delta p}{\rho}\right) = -\frac{1}{\tau}\frac{\partial^2}{\partial y^2}\left(\frac{\delta p}{\rho}\right), \tag{27}$$

$$\frac{\partial}{\partial t}\nabla^2 u_y = -\frac{1}{\tau}\frac{\partial^2 u_y}{\partial y^2}. \tag{28}$$

At this point it is natural to look for plane-wave solutions of the type discussed in Sec. I B. However, plane-wave solutions of (25) and (26), subject to boundary conditions (11) and (12), lead to exactly the same dispersion relationship as before, and hence to waves that are damped out on a time scale of $t_d \sim \tau$. Yet we know from the experiments (described in Sec. IV) that the damping time for waves in an insulating box is an order of magnitude greater than τ. Thus we are led to the surprising conclusion that simple plane-wave solutions are not observed when the walls are nonconducting. To explain this phenomenon, we must first determine the manner in which the current paths close within the fluid.

The simplest case to analyze is the weak-field, shallow-water limit, and so we start with this. Here u_x is independent of depth to leading order in kh and can be written as $u_x = u_0(t)\cos(\pi x/L)$. From (3), we have $\nabla^2 V=0$ and the boundary condition $\mathbf{J}\cdot\mathbf{n}=0$ demands

$$\frac{\partial V}{\partial z} = u_0 B_0 \cos(\pi x/L), \quad z = \pm w/2;$$

$$\frac{\partial V}{\partial x} = 0, \quad x = \pm L/2.$$

The solution for V is

$$\frac{V}{u_0 B_0} = \frac{2z}{\pi} - \frac{4}{\pi}\sum_{n=1}^{\infty}\frac{(-1)^n}{(2n)^2-1}\frac{\sinh(k_n z)\cos(k_n x)}{k_n \cosh(k_n w/2)}, \tag{29}$$

where $k_n = 2n\pi/L$. [It is readily confirmed that (29) satisfies Laplace's equation and the boundary conditions.] The corresponding current distribution can be found from Eq. (1) and used to calculate the net Ohmic dissipation. It turns out to be

$$D_J = \int (\mathbf{J}^2/\sigma)dV = \frac{1}{2}\sigma B_0^2 u_o^2 (Lwh) \times \left(\frac{4}{\pi}\right)^2 \sum_{n=1}^{\infty}\frac{1}{[(2n)^2-1]^2}\left(1 - \frac{\tanh p_n}{p_n}\right), \tag{30}$$

where $p_n = n\pi w/L$. This may be compared with the equivalent result for perfectly conducting walls,

$$D_J^* = \int (\mathbf{J}^2/\sigma)dV = \frac{1}{2}\sigma B_0^2 u_o^2 (Lwh),$$

from which we conclude that the Joule dissipation is reduced by a factor of

$$\frac{D_J}{D_J^*} = \left(\frac{4}{\pi}\right)^2 \sum_{n=1}^{\infty}\frac{1}{[(2n)^2-1]^2}\left(1 - \frac{\tanh p_n}{p_n}\right). \tag{31}$$

Now, for a weakly damped system whose amplitude decays as $\exp(-t/t_d)$, we have

$$\frac{2}{t_d} = \frac{\text{Dissipation averaged over a cycle}}{\text{Total energy during the cycle}}. \tag{32}$$

Moreover, $t_d = 2\tau$ for perfectly conducting walls in the shallow-water limit. It follows that, for nonconducting walls,

$$\frac{\tau}{t_d}=\frac{1}{2}\left(\frac{4}{\pi}\right)^2\sum_{n=1}^{\infty}\frac{1}{[(2n)^2-1]^2}\left(1-\frac{\tanh p_n}{p_n}\right). \tag{33}$$

Let us write this as $t_d=A_0\tau$, where A_0 is a function of w/L only. In our experiment, where $w/L=4/15$, we find $A_0=53$. This large value of A_0 is a little surprising, but it arises from the fact that the magnitude of $\mathbf{J}$ is considerably reduced when the current is forced to return within the fluid. Now, Eq. (33) applies only in the weak-field, shallow-water limit. For strong damping the velocity field is no longer harmonic and so we cannot justify the assumption that $u_x \sim \cos(\pi x/L)$. However, the damping in our experiments is usually weak for nonconducting walls, largely because A_0 is large. Thus, we might expect (33) to apply even at moderate-to high-field strengths. Equation (33) is not a good approximation, however, if we move outside the shallow-water limit. This is because D_J is a function of u_x only, while the kinetic energy has contributions from both u_x and u_y. As we move away from the shallow-water limit the relative contribution from u_y rises and, hence, because of (32), t_d also increases. To allow for this we write

$$t_d=A(kh,w/L)\tau=C_dA_0(w/L)\tau, \tag{34}$$

where A_0 is given by (33). The coefficient C_d is equal to unity in the shallow-water limit and, from the discussion above, it is expected to rise monotonically with depth as we move towards the deep-water limit.

It remains to incorporate the effects of viscosity. There are two kinds of boundary layers to be considered: the conventional viscous layers on the sidewalls and the Hartmann layer on the base. Consider first the side layers. Since these are thin we may assume that, at any one location, the x dependence of the core velocity is unimportant and so the side layers may be approximated by the model problem in which a uniform flow oscillates over the boundary. That is to say $u_x=u(z)\exp(j\varpi t)$, where $u(z)$ is constant and equal to u_∞ away from the boundaries. The corresponding boundary layer thickness is $\delta_\varpi=\sqrt{2\nu/\varpi}$ and the dissipation per unit area of the boundary layer, averaged over a cycle, is readily shown to be

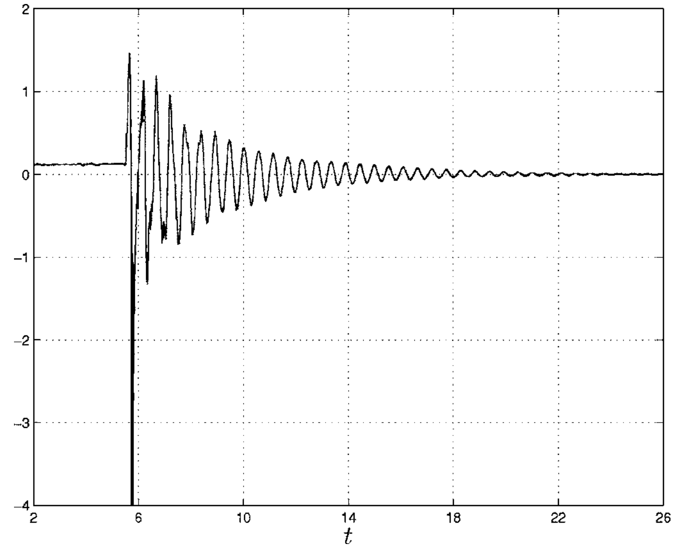

FIG. 6. Amplitude of the surface wave (mm) as a function of time (s) for $N_0=0.17$, measured in a cavity with electrically conducting (copper) walls. The downward spike corresponds to the point when the box is displaced for the creation of the wave.

$$\overline{D_\varpi}=\tfrac{1}{2}\rho\nu u_\infty^2/\delta_\varpi. \tag{35}$$

The Hartmann layer on the base of the pool is a combination of a conventional Hartmann layer and the oscillating boundary layer described above. Since this layer is very thin, we may once again use the approximation of a uniform flow oscillating over the boundary. The governing equation is then

$$\frac{\partial u_x}{\partial t}=-\frac{u_x}{\tau}+\nu\frac{\partial^2 u_x}{\partial y^2},$$

which yields a boundary layer thickness of

$$\delta=(\delta_H^{-4}+4\delta_\varpi^{-4})^{1/4},$$

where $\delta_H=\sqrt{\nu\tau}$ is the conventional Hartmann layer thickness. (See, for example, Muller and Buhler.[6]) It is readily confirmed that the dissipation per unit area of this Hartmann layer is, averaged over a cycle,

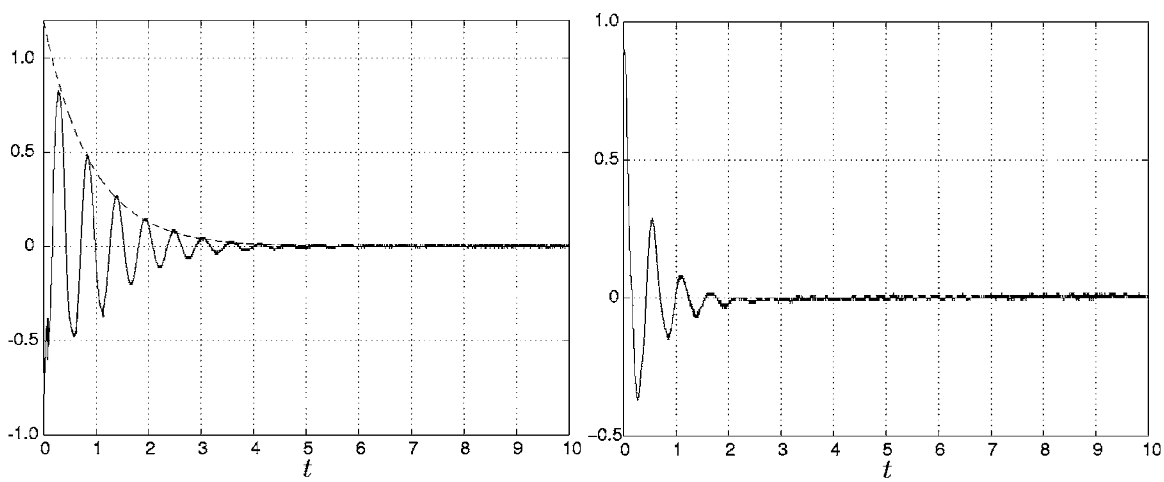

FIG. 7. Measured evolution of the surface perturbation (mm) for $N_0=1.60$ (left) and $N_0=2.2$ (right) in an electrically conducting box.

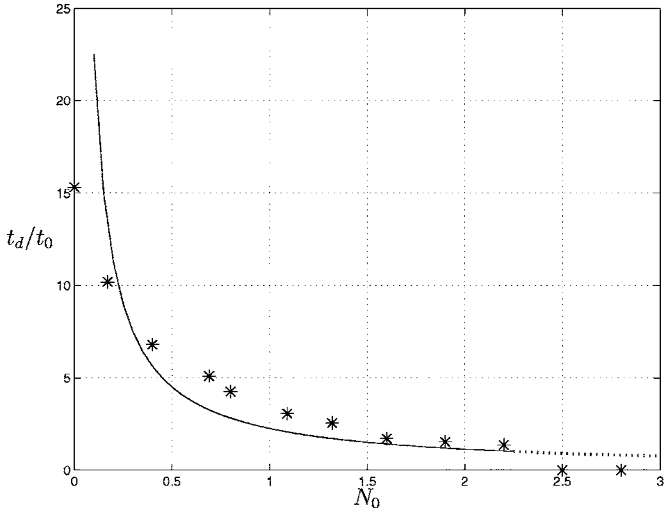

FIG. 8. A comparison of the experimentally obtained magnetic damping times (normalized with respect to the natural period of oscillation in the absence of a magnetic field, t_0) for an electrically conducting box, with the theoretical estimate (18). The fluid depth is $h=0.03$ m, and $k=20.9$ m^{-1}. The dotted line corresponds to the region where the wave is arrested by the magnetic field (no oscillations). Note that $N_0=(\varpi_0\tau)^{-1}$.

$$\overline{D_H}=\frac{\rho\nu u_\infty^2}{2\sqrt{2}\delta_H}\{1+[1+(\varpi\tau)^2]^{1/2}\}^{1/2}. \tag{36}$$

From Eqs. (30), (35), and (36), we can estimate the total dissipation averaged over a cycle in the shallow-water limit. On substituting into (32), we then obtain the corresponding value of t_d. We find

$$\frac{\tau}{t_d}=\frac{1}{A_0}+\frac{\mathrm{Re}^{1/2}}{\sqrt{2}Ha^2}+\frac{w}{2\sqrt{2}h}\frac{\{1+[1+(\varpi\tau)^2]^{1/2}\}^{1/2}}{Ha}, \tag{37}$$

where $\mathrm{Re}=w^2\varpi/\nu$. The terms on the right-hand side correspond to bulk Ohmic dissipation, viscous sidewall dissipation, and Hartmann layer dissipation, respectively. At high Ha, which is typical of our experiments, the first term is dominant.

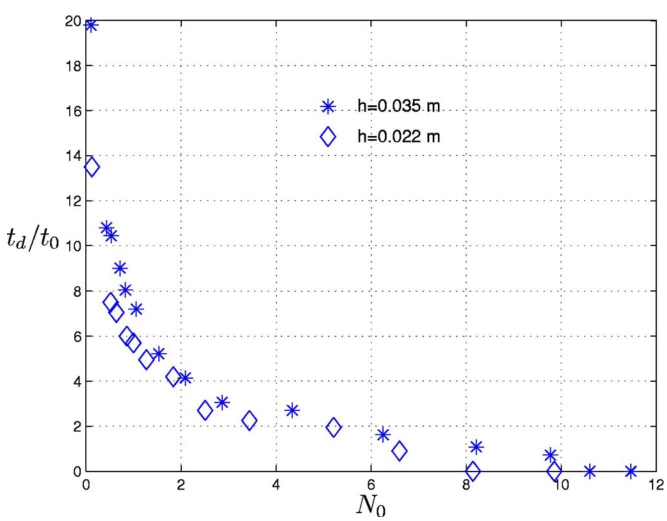

FIG. 9. Measured magnetic damping times normalized with respect to the natural time of oscillation when $B_0=0$, t_0, plotted as a function of N_0, for an electrically insulating cavity.

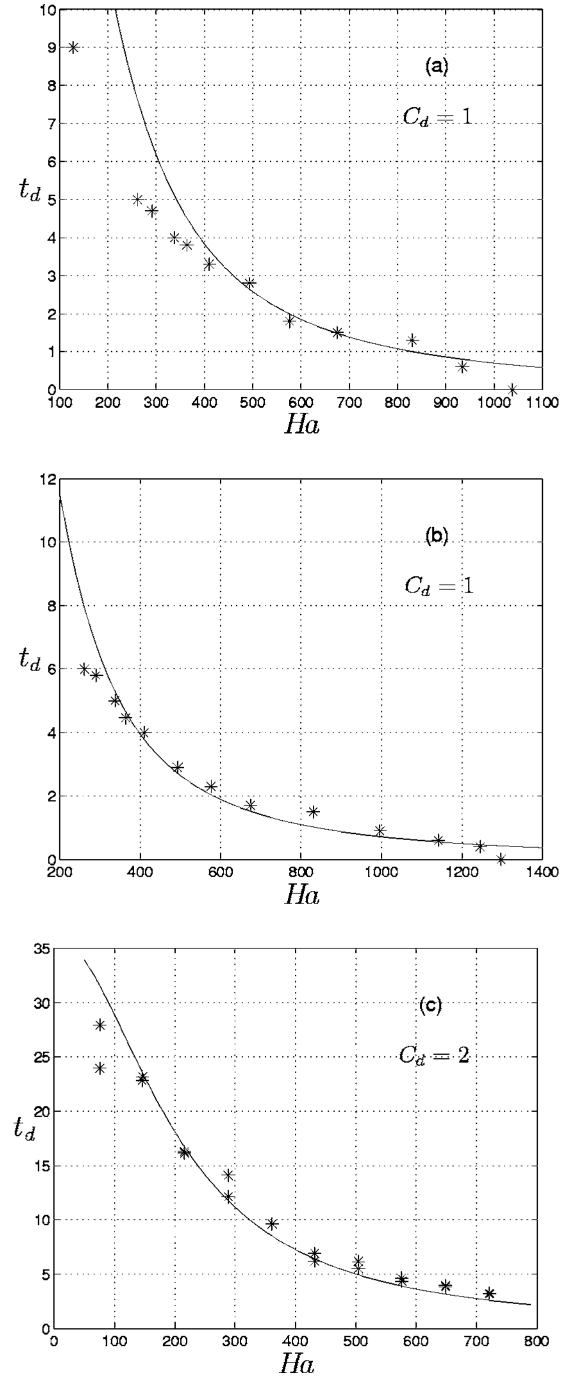

FIG. 10. Experimentally measured damping times (s) for insulating walls as a function of the Hartmann number for (a) $h=0.022$ m, (b) $h=0.035$ m, and (c) $h=0.08$ m. The superposed curves represent the relations obtained from theory, with $C_d=1$ for $h=0.02$ and 0.035 m and $C_d=2$ for $h=0.08$ m.

III. THE EXPERIMENT

A schematic of the experimental setup is given in Fig. 5. An open box of internal dimension $150\times40\times80$ mm contains mercury and sits in an imposed vertical magnetic field. Two different boxes are used. One is a box made of highly

TABLE I. Table showing the typical magnetic fields, B_0 (T) imposed on a fluid layer of depth 35 mm in an electrically conducting box, the corresponding interaction parameter, N_0, the Hartmann number, Ha, and the measured damping time, t_d (s).

B_0	N_0	Ha	t_d (s)
0.158	0.17	164.0	6.0
0.32	0.69	330.95	3.0
0.40	1.09	415.96	1.8
0.49	1.60	503.96	1.0
0.57	2.20	590.95	0.8
0.595	2.40	617.22	≈ 0

TABLE II. Table showing the range of operating parameters B_0 (T), N_0, Ha, and t_d (s) for the case of an electrically insulating box with a fluid layer of depth 35 mm.

B_0	N_0	Ha	t_d (s)
0.252	0.43	261.55	6.0
0.35	0.83	363.26	4.47
0.475	1.53	493.0	2.9
0.65	2.87	674.63	1.7
0.96	6.26	996.38	0.9
1.20	9.78	1245.48	0.4
1.30	11.47	1349.27	≈ 0

conducting copper, with wall thickness 10 mm, and the other is made of electrically insulating Plexiglas (polymethyl methacrylate).

A standing wave is created at the free surface of the fluid by imparting a horizontal (x) acceleration to the box by mechanical means against a vertical stop. The maximum angle, θ, that the free surface of the liquid makes with the horizontal, is related to the acceleration imparted to the box, a, by $\tan\theta = a/g$. By controlling a/g, it was possible to ensure that θ remained small at all times.

The perturbations of the free surface are measured by an optical displacement sensor. A 1 mJ, 670 nm (red) laser, mounted approximately 200 mm from the free surface of the fluid, shines a beam onto the surface. The reflected beam is received by a position detector situated beside the laser source, which converts the position data into the actual distance of the fluid surface from the sensor. This provides an effective nonintrusive means of measuring free surface perturbations in an opaque fluid to a resolution of 0.01 mm. A maximum sampling rate of 1000 s^{-1} ensures that a wave of frequency $\sim$2 Hz, and other harmonics (if present), are captured without aliasing errors.

IV. THE RESULTS

We shall first consider magnetic damping in an electrically conducting box. Figure 6 shows surface oscillations (in mm) for $N_0 = (\varpi_0 \tau)^{-1} = 0.17$ recorded in a 30 mm deep fluid pool. The downward spike observed at $t \approx 6$ s corresponds to the instant when the box is subject to a horizontal impulse. The wave soon settles down to a regular sinusoidal pattern. Two seconds after the initial impulse, the surface displacement has an exponentially decaying profile, enabling the measurement of a decay time constant. In Fig. 7, the data measured immediately after the wave is created are presented for $N_0 = 1.6$ and $N_0 = 2.2$. The damping times decrease with increasing N, signifying the dominant effect of Joule dissipation, and when $N_0 = 2.2$, the wave is brought to rest after only three oscillations. A further increase of the field strength results in total suppression of the wave (critical damping).

Figure 8 compares the experimentally obtained damping times with the theoretical solution (18) for the case $h = 0.03$ m, $k = 20.9$ m^{-1} ($kh \approx 0.6$). The comparison is favorable. Note that the critical value of N_0 at which ϖ_r goes to zero, is close to the theoretical value of 2.25.

Figure 9 shows the damping time as a function of N_0, measured in an electrically insulating vessel. To achieve the same damping times as those for a conducting vessel, the interaction parameters needed are almost one order of magnitude higher. Finally Fig. 10 shows the damping time t_d plotted against Ha for the cases $h = 22$ mm, $h = 35$ mm, and $h = 80$ mm. (In the third case, $h = 80$ mm, there was some nonuniformity in the imposed magnetic field.) Note that $h = 22$ mm and $h = 35$ mm are close to the shallow-water limit ($kh = 0.46, 0.73$), and so we may make a direct comparison with the theoretical estimate (37). The comparison is excellent for the case $h = 35$ mm, and reasonable for $h = 22$ mm, though it slightly underestimates the damping time for weak fields. For $h = 80$ mm, we are outside the shallow-water regime and so we have replaced A_0 in (37) with $C_d A_0$ in accordance with (34). We expect $C_d > 1$ and indeed taking $C_d = 2$ gives an excellent fit to the data.

Tables I–III give the typical values of the external magnetic field imposed on fluid layers in conducting and insulating cavities, the corresponding interaction parameters and Hartmann numbers, and the measured damping times in these experiments.

V. DISCUSSION

It is encouraging that the scaling predicted by Eq. (37) is borne out by the experiments. The measurements made close to the shallow-water limit ($h = 22$ mm and $h = 35$ mm) are particularly important as the corresponding theoretical esti-

TABLE III. Table showing the range of operating parameters B_0 (T), N_0, Ha, and t_d (s) in an electrically insulating box with a fluid layer of depth 80 mm.

B_0	N_0	Ha	t_d (s)
0.136	0.107	143.56	22.99
0.204	0.241	215.34	16.22
0.272	0.429	287.12	13.07
0.340	0.670	358.90	9.62
0.408	0.964	430.68	6.55
0.476	1.313	502.46	5.84
0.544	1.715	574.24	4.49
0.612	2.170	646.03	3.90
0.680	2.679	717.81	3.21

mate of t_d contains no adjustable parameter, so the close correspondence with theory provides convincing proof that Eq. (37) is correct.

From a practical point of view, the important point is that, when the container walls are insulating, the time scale for magnetic damping is no longer τ, but rather an order of magnitude higher. This is important since insulating walls represent the most common situation in metallurgical applications.

ACKNOWLEDGMENTS

One of the authors (B.S.) was sponsored by a one-year CNRS/ARCELOR research fellowship held at the Laboratoire CNRS-EPM at Grenoble, France. The authors would like to thank an anonymous referee for making several useful suggestions.

[1] P. A. Davidson, "Magnetohydrodynamics in materials processing," Annu. Rev. Fluid Mech. **31**, 273 (1999).
[2] P. A. Davidson, *An Introduction to Magnetohydrodynamics* (Cambridge University Press, Cambridge, 2001).
[3] L. E. Fraenkel, "A shallow-liquid theory in magnetohydrodynamics," J. Fluid Mech. **7**, 81 (1959).
[4] P. Rivat, J. Etay, and M. Garnier, "Stabilization of a surface wave by a magnetic field," Eur. J. Mech. B/Fluids **10**, 537 (1991).
[5] A. Ya. Shishkov, "Wave processes at the surface of a magnetohydrodynamically buoyed fluid," Magnetohydrodynamics (N.Y.) **28**, 368 (1992).
[6] U. Muller and L. Buhler, *Magnetohydrodynamics in Channels and Containers* (Springer, Berlin, 2001).